RSC Advances

ROYAL SOCIETY OF CHEMISTRY

www.rsc.org/advances

Amidic C-N bond cleavage of isatin: Chemoselective synthesis of pyrrolo[2,3,4-*kl*]acridin-1-ones using Ag NPs decorated rGO composite as an efficient and recoverable catalyst under microwave irradiation

Anshu Dandia,*[a] Amit Sharma,[a] Vijay Parewa,[a] Begraj Kumawat,[a] Kuldeep S. Rathore[b] and Amit Sharma[b]

[a]Centre of Advanced Studies, Department of Chemistry, University of Rajasthan, Jaipur, India.

[b]Semiconductor and Polymer Science Laboratory, Department of Physics, University of Rajasthan, Jaipur, India.

E-mail[a]: dranshudandia@yahoo.co.in E-mail[b]: kuldeep_ssr@yahoo.com

ABSTRACT

We have developed a facile approach for the synthesis of Ag NPs decorated reduced graphene oxide (Ag NPs/rGO) composite *via* novel chemical route. This synthetic protocol coalesce protection, reduction and functionalization of graphene oxide in one step. The as prepared Ag NPs/rGO composite has been characterized by TEM, XRD, SEM, XPS, EDX, UV–Vis, CV, Raman and FT-IR spectra. The results showed that plenty of Ag NPs (~28 nm) are homogeneously distributed onto the surface of rGO. Further, catalytic applications of this fascinating nanomaterial have been utilized for the chemoselective synthesis of pyrrolo[2,3,4-*kl*]acridin-1-ones *via* ring-opening sequence or amidic C-N bond cleavage of isatin. The Ag NPs/rGO composite possesses assets of both Ag NPs and graphene based material, thus, provided enhanced surface acidity with good dispersion capability that usually lacks in Ag NPs alone. After completion of catalytic reaction, Ag NPs/rGO composite could be easily recovered by simple filtration and recycled for 7 times without significant loss in catalytic activity. The recycling and hot-filtration experiments proved the high stability and no leaching of the synthesized nanomaterial during the catalytic process. Furthermore, proposed protocol showed excellent results in terms of green metric parameters confirming the effectiveness and profound appeal of protocol.

KEYWORDS: Pyrrolo[2,3,4-*kl*]acridin-1-ones, Microwave irradiation, Ag NPs/rGO composite, Chemoselective synthesis, Green metrics.

1. INTODUCTION

Pyrroles are found in a wide variety of bioactive natural products and compounds of current therapeutic interest. These compounds exhibit remarkable biological properties such as antimicrobial, antioxidant, anti-HIV and antifungal activity, cyclooxygenase-2 (COX-2) inhibitors, antagonists of the gonadotropin-releasing hormone (GnRH) receptor, etc.[1] Their potential applications are also explored in the field of advanced optoelectronic materials.[2]

Besides, acridine nuclei substituted with various heterocyclic rings is center of interest in medical sciences. It founds in an intriguing array of pharmaceutically and naturally occurring products exhibiting a wide spectrum of biological and therapeutic properties. These moieties show antibacterial, trypanocidal, and antimalarial activities.[3] Some drugs possessing acridine nuclei also inhibit the growth of cancerous cells via binding to DNA and act as potent anticancer drugs.[4] Furthermore, acridine derivatives play particular roles in biocatalysis as they serve as haptens of catalytic antibody 9D9.[5]

A pyrroloacridine nucleus which accumulates pyrrole as well as acridine moieties integrates the properties of both and their synergism in a single nucleus results in the formation of some worthwhile molecules from the biological point of view (Fig. 1). Derivatives of pyrroloacridine exhibit promising biological activities such as anthelmintic and anticancer activity.[6] Further, pyrroloacridine compounds are found as the tetracyclic cores in metabolites from marine sources such as plakinidines A–C and alpkinidines.[7]

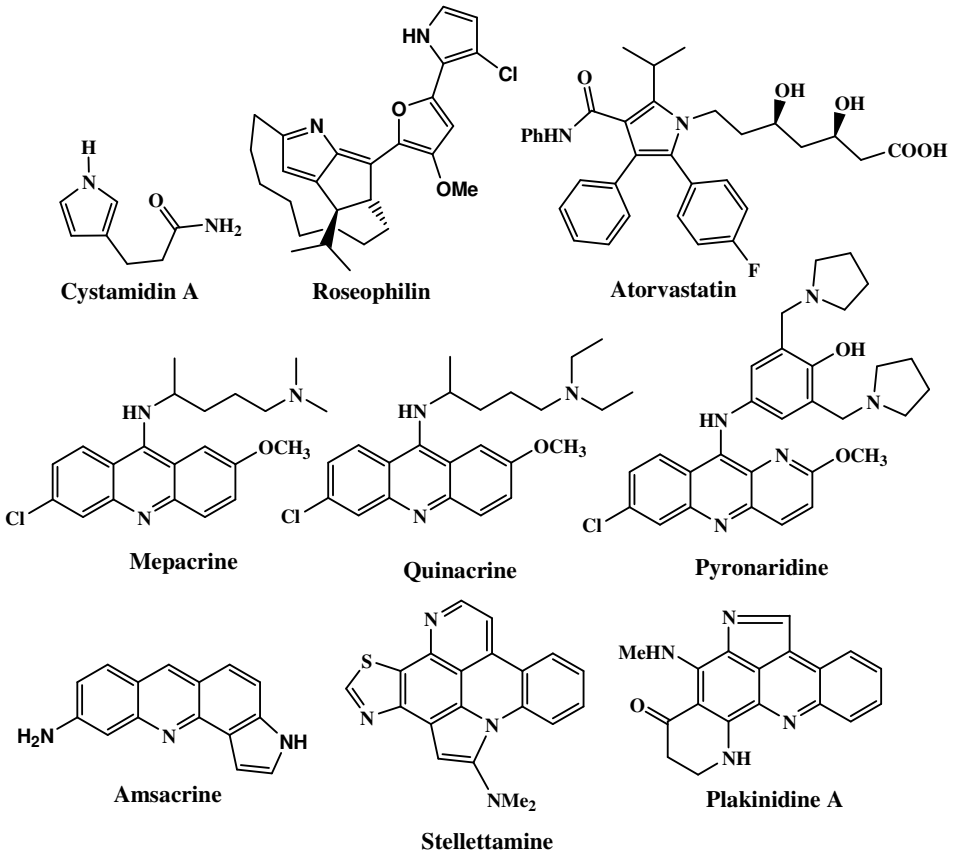

Fig. 1 Several representative bioactive pyrroles and acridines.

These examples emphasize the vital importance of pyrroloacridines as key pharmacophores in bioactive molecules. But as illustrated in Fig. 2, only a few reports are available for the synthesis of pyrroloacridine skeletons: (a) multi step synthesis from proflavine;[8a] (b) condensation of 1,3-cyclohexanedione with 2-amino-2'-acetamido-acetophenone;[8b] (c) condensation of 4,5,6,7-tetrahydroindol-4-ones with anthranilonitrile;[8c] (d) oxidation of 2-acetyl-3'-nitrodiphenylamine;[8d] (e) condensation of 5-amino-2-methylindole with o-halobenzoic acids,[8e] and (f) reactions of isatins with enaminones[8f-h].

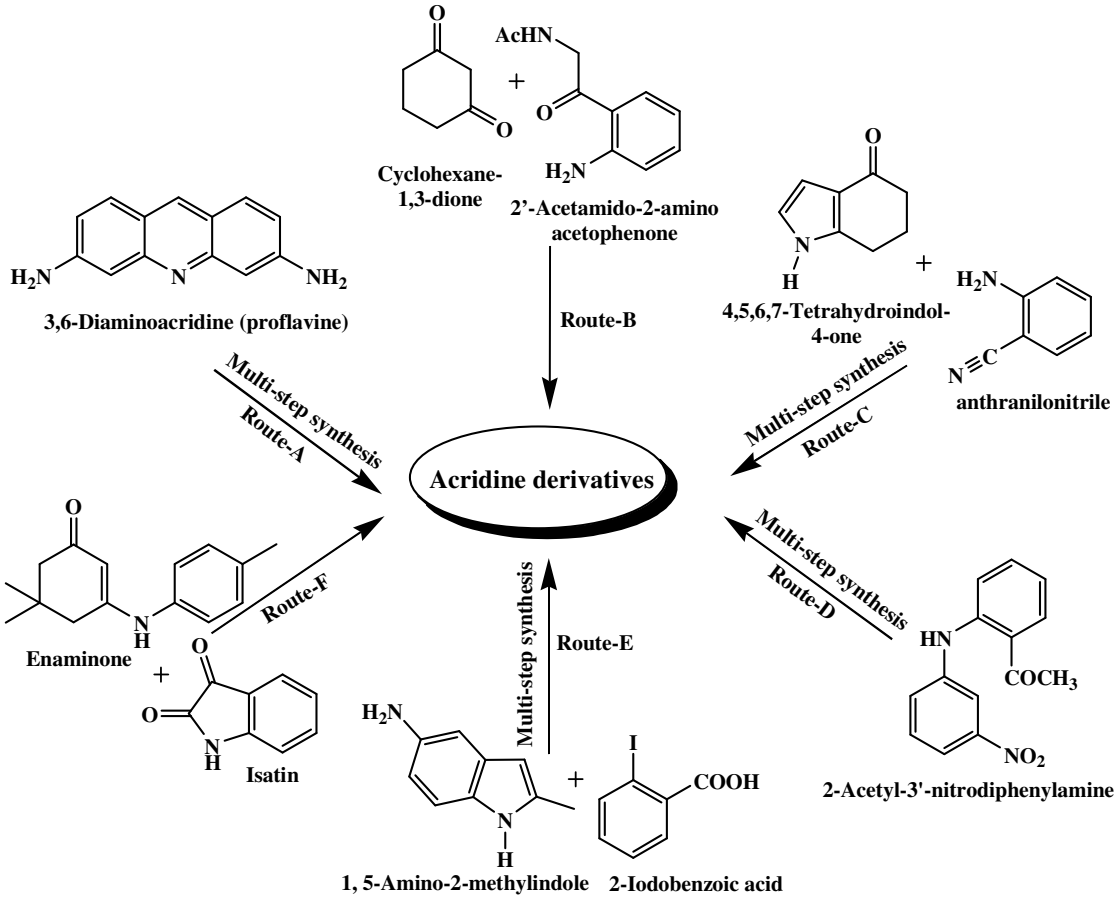

Fig. 2 Previously used methods for the synthesis of acridine derivatives.

However, these methodologies suffer from some shortcomings due to their restricted efficacy i.e. multistep processes,[8a,8c-e] use of corrosive and toxic reagents,[8a-e] high reaction temperature, long reaction time, non-compatible solvents and low yields,[8b,8f-g] unavailable starting materials,[8f-h] etc. Moreover, the recovery of used catalyts is not so good and has reduced turn over frequency (TOF) which adversely affects the economic as well as the ecofriendly nature of these reported methodologies. Although, deliberated modifications have been documented by using ionic liquid,[9] but it requires tedious preparation methods.

Moreover, their environmental safety is still arguable due to their corrosive, non bio-degradable and toxic nature.[10] Further, the substrate applicability of the engaged protocol was limited.[9] These downsides inspired us to reinvestigate this transformation.

Improvement in sustainability of chemical processes can efficiently be achieved by means of process intensification through catalysis.[11] In this direction, the one-pot procedures linked with some competent catalytic systems have become a vital area of research in organic chemistry since they allow the lessening of energy consuming steps such as separation, identification and purification of intermediates.[12] Also, they improve atom economy and lower the E factors and raw materials consumption.[13] Considering this model, challenges for one-pot transformations are foccused on the design of highly selective catalysts with well-recognised isolated active sites.

Recently, the use of carbon nanomaterials in catalysis has grown importance and dominated advances in nanoscience.[14] Among them nanosheets has opened a new route for the use of two dimensional carbon materials as catalytic supports due to their oxidative resistance for chemical reactions, high electrical and thermal conductivities, good water-dispersion, great mechanical strength, easy availability in bulk quantities, huge specific surface area and presence of reactive oxygen functional groups i.e. hydroxy, carbonyl, carboxylic acid group, etc.[15] Taking full advantage of the surface functional groups, as well as large specific surface area and stability, graphene oxide (GO) nanosheetshas allowed researchers to design and develop countless combinations of GO-based materials.[16] Toward this end, recent studies have endeavored to anchor noble metallic nanoparticles on GO nanosheets for enhanced physical and chemical properties.[17]

Among the noble metals, silver nanoparticles have become the focus of intensive research due to their catalytic properties for some important organic reactions.[18] Further, silver nanoparticles are also studied for the catalytic reactions involving activation of carbonyl group.[19] Additionally, they are promising candidate for optical, electrical and electronic applications.[20] Currently, most of the applications of silver nanoparticles are explored as antibacterial agents in biotechnology, bioengineering, textile engineering, water treatment, and silver-based consumer products.[21] A desire to exploit the unique catalytic properties of Ag NPs led us to synthesize Ag NPs on GO sheets. We believe that the hybrid material of Ag NPs, where a layered material like GO is used as active support, can provide

large surface area and stability with good dispersion capability that usually lacks in Ag NPs alone and thus enhance its catalytic activity.

Therefore, in the course of our research efforts for the development of efficient methods for heterocyclic synthesis and nanocatalysts preparation,[22] we wish to report herein the synthesis of highly stable and recyclable Ag NPs/rGO composite and its catalytic applications for the chemoselective synthesis of pyrrolo[2,3,4-*kl*]acridin-1-ones by one pot reaction of dimedone, various anilines and isatins *via* ring opening sequence and intramolecular cyclization under microwave irradiation (Scheme 1). Literature survey reveals that similar type of reaction succession of 1,3-diketones, aromatic amines and isatins capitulated different type of products instead of pyrrolo[2,3,4-*kl*]acridin-1-ones.[23] This fact resulted in our enthusiasm for exclusive formation of the pyrrolo[2,3,4-*kl*]acridin-1-one derivatives.

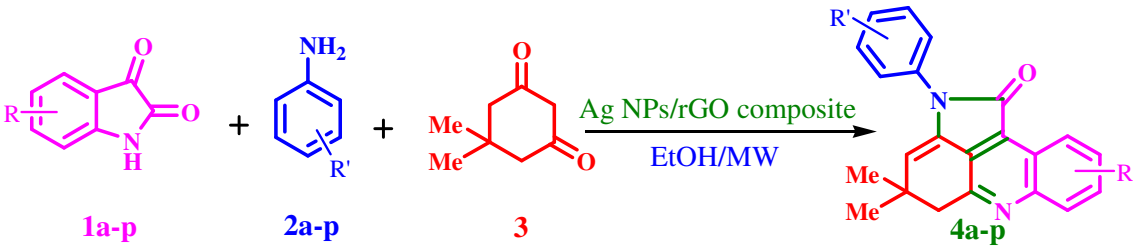

Scheme 1: Ag NPs/rGO composite catalyzed synthesis of pyrrolo[2,3,4-*kl*]acridin-1-ones.

2. RESULTS AND DISCUSSION

2.1. Synthesis and characterization of catalyst

In present study, we combined the concepts of Ag NPs (high catalytic activity) with GO (large surface area and good electrical conductivity). The Ag NPs/rGO composite was synthesized by an effective and fast one-pot chemical route incorporating the simultaneous reduction GO and preparation of Ag NPs on its surface. The advantages of this method lies in its simplicity, cost effectiveness, environment friendliness, easier scaling up for large scale synthesis while avoiding the use of high pressure, temperature and toxic chemicals. The morphology and structure of the prepared Ag NPs/rGO composite were characterized by TEM, XRD, SEM, XPS, EDX, UV–Vis, Cyclic voltammetery, Raman and FT-IR spectra, which confirmed the successful preparation of the Ag NPs/rGO composite.

Fig. 3 shows the XRD patterns of (a) graphene oxide, (b) reduced graphene oxide and (c) Ag NPs/rGO composite. In Fig. 3a the characteristic (001) diffraction peak of graphene oxide is clearly observed. In the XRD pattern of reduced graphene oxide, the characteristic

(002) diffraction peak of rGO is appeared and characteristic peak of GO does not reappear which reveals that the reduction of GO sheets has been successfully accomplished (Fig. 3b). The successful modification of Ag NPs on rGO sheets is indicated by the XRD pattern of Ag NPs on rGO sheets (Fig. 3c). Using Scherrer's formula, the particle crystalline size of Ag NPs in Ag NPs/rGO composite was calculated to be 20 nm.

Furthermore, apparent diffraction peaks of graphene oxide (Fig. 3a) were not observed in the as-synthesized composites. It might be due to the facts that- (i) the content of graphene oxide is relatively lower and diffraction signals of silver cover up those of the carbon sheets; (ii) the exfoliation of graphene oxide.[24]

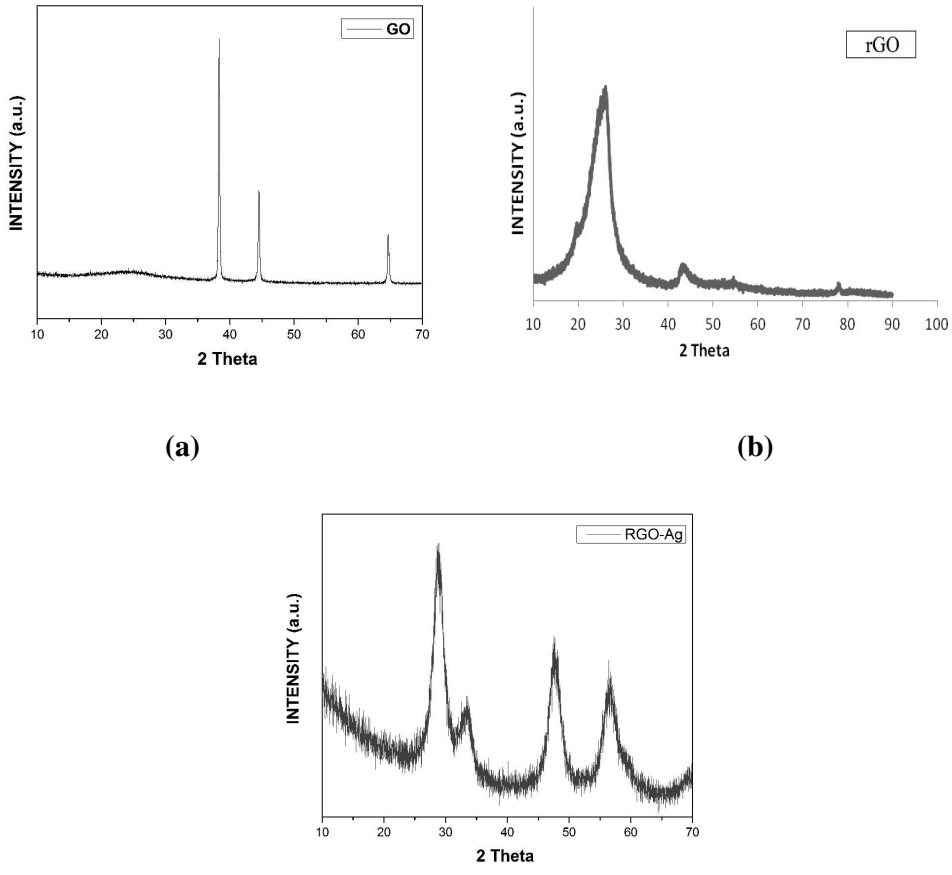

Fig. 3 XRD patterns of (a) graphene oxide, (b) reduced graphene oxide and (c) Ag NPs/rGO composite.

Fig. 4 shows the typical SEM images of as-prepared (a) graphene oxide, (b) reduced graphene oxide and (c) Ag NPs/rGO composite. It is clearly seen in Fig. 4a that the surface of GO sheets displayed a typical crumpled and wrinkled behavior due to the deformation upon

exfoliation and restacking processes. The rGO nanosheets are layer structured having irregular overlapping of sheets and illustrate further exfoliation during the reduction of GO into rGO (Fig. 4b). It can be observed from Fig. 4c that Ag NPs are well decorated on rGO sheets.

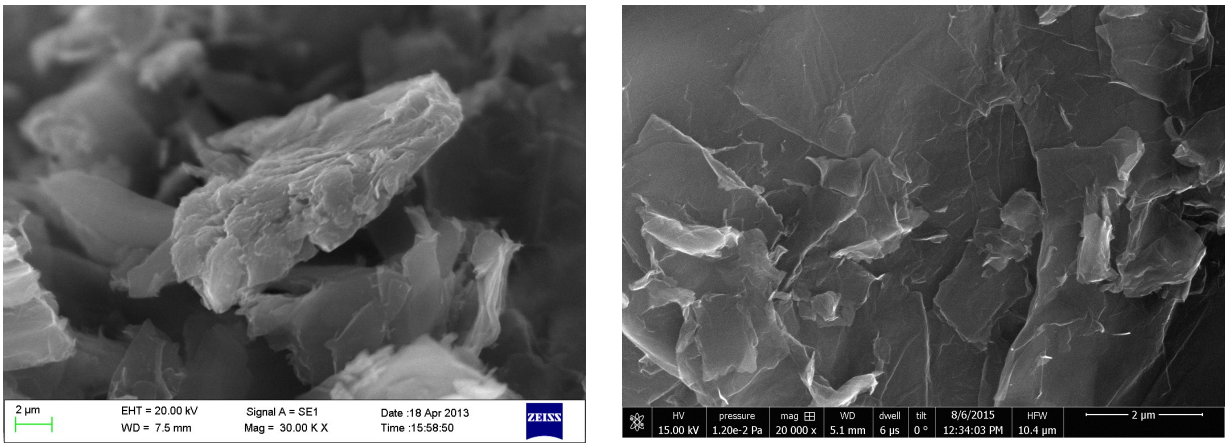

(a) **(b)**

(c)

Fig. 4 SEM image of as-prepared (a) graphene oxide, (b) reduced graphene oxide and (c) Ag NPs/rGO composite.

Fig. 5a shows the typical TEM image of the Ag NPs/rGO composite, in which a number of small black dots are observed on the rGO sheets. These dots are approximately 28 nm in size and irregular in shape. It demonstrates the formation of Ag NPs well decorated on rGO sheet. For comparison, we also prepared Ag NPs separately from same procedure but without GO and the TEM image is shown in Fig. 5b. Generally, the aggregation of Ag NPs leads to a significantly decreased surface area, which means, if un-protected, Ag NPs

aggregate spontaneously. In this experiment, the oxygen-containing groups on GO sheets supply chemical active centers for Ag deposition. Ag NPs can be deposited on both sides of these sheets (as revealed by SEM and TEM images). Ag NPs are well separated from each other and distributed randomly on the rGO sheets. Highly dispersed Ag NPs on supports with larger surface area are beneficial to improve the catalytic activity.

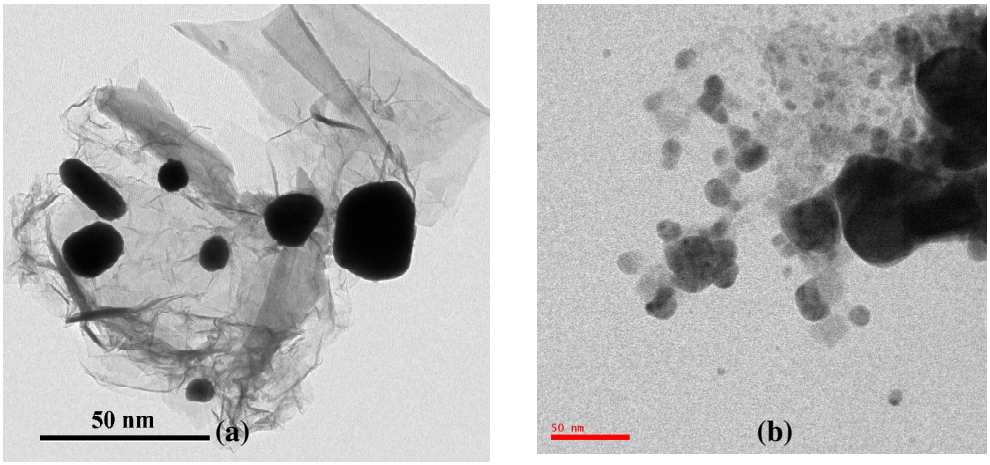

Fig. 5 TEM image of as-prepared (a) Ag NPs/rGO composite and (b) Ag NPs.

The reduction of GO and formation of rGO or Ag NPs/rGO composite was further confirmed by X-ray photoelectron spectroscopic (XPS) measurements (Fig. 6). The deconvoluted C 1s spectra of GO shows three peaks at 284.1, 285.0 and 286.1 eV which corresponds to the C=C/C–C, C–O and C(epoxy)/ C=O functionalities respectively (Fig. 6a).[25a,28c] While a notable decrease in the intensity of the peaks of C–O and C(epoxy)/ C=O functionalities in the C1s XPS spectra of rGO (Fig. 6b) and Ag NPs/rGO composite (Fig. 6c) is observed which confirms the efficient reduction of GO. In the Ag 3d XPS core level spectra of Ag NPs/rGO composite, the signals at 368.1 and 374.1 eV are observed due to Ag $3d_{5/2}$ and Ag $3d_{3/2}$ respectively which suggests the formation of metallic Ag NPs on the rGO nanosheets (Fig. 6d).[25c,d] These results confirm the successful reduction of GO and formation of Ag NPs on rGO sheets.

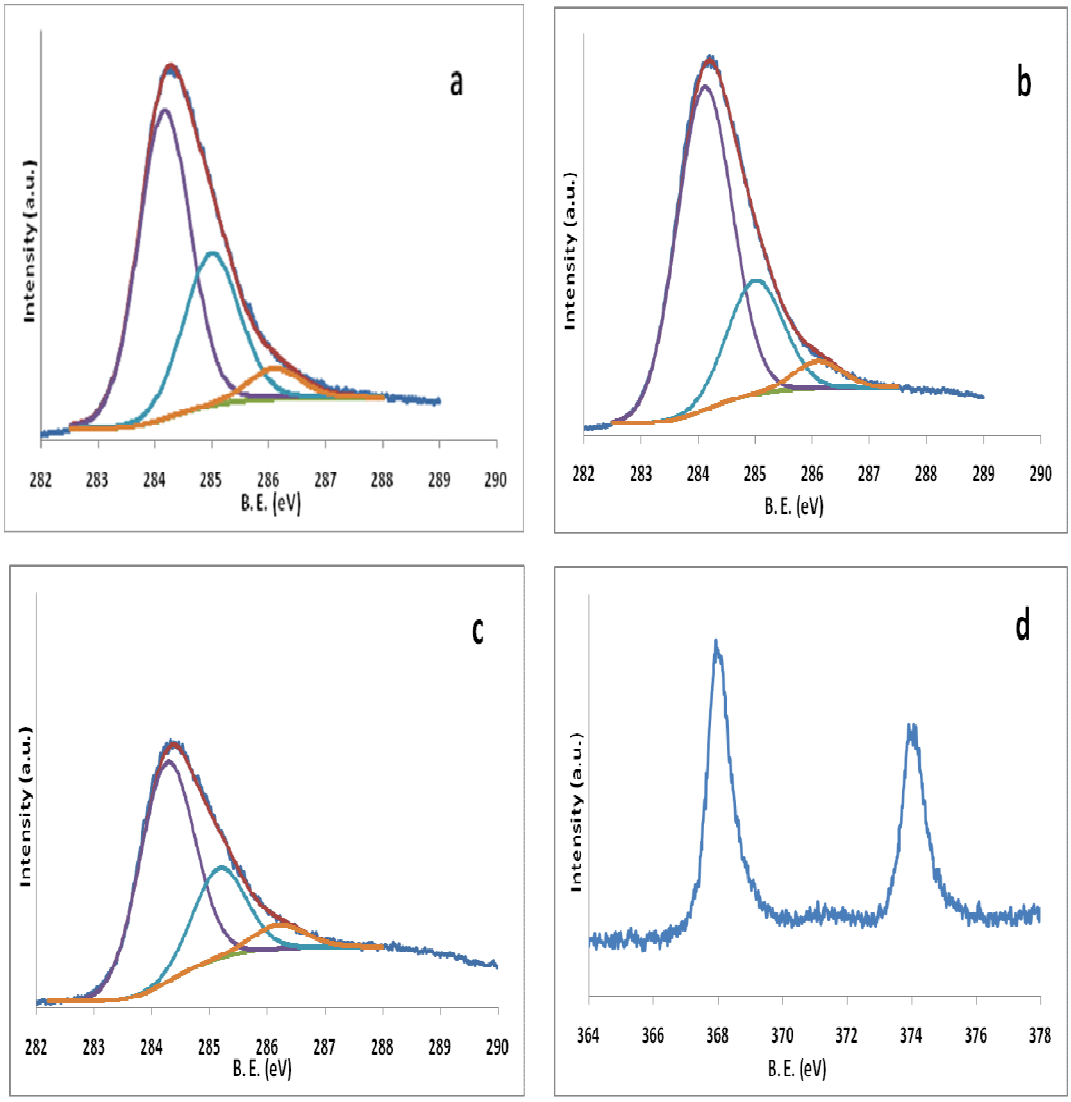

Fig. 6 C 1s XPS spectra of (a) GO and (b) rGO and (c) Ag NPs/rGO composite, and (d) Ag 3d XPS spectrum of Ag NPs/rGO composite.

The energy-dispersive X-ray (EDX) spectrum of graphene oxide, reduced graphene oxide and Ag NPs/rGO composite is shown in Fig. 7. The EDX analysis revealed that the composition of GO sheets mostly consisted of C and O (70 wt% C and 30 wt% O) (Fig. 7a) and show quite good or almost similar results as compared to reported Hummers or modified Hummers method in which $KMnO_4$ was utilized as an oxidizing agent.[26] These analytical results prove the oxidizing efficiency of our protocol since we have not used $KMnO_4$ during the oxidation of graphite flakes. From the EDX spectrum of rGO (Fig. 7b), the decreased oxygen content (81 wt% C and 19 wt% O) proves the successful reduction of GO into rGO. Fig. 7c confirms the presence of C, O, and Ag in synthesized Ag NPs/rGO composite (45

wt% C, 9 wt% O and 46 wt% Ag). The signals of C and O elements originated from the rGO sheets and signals of Ag element resulted from the decorated sliver NPs.

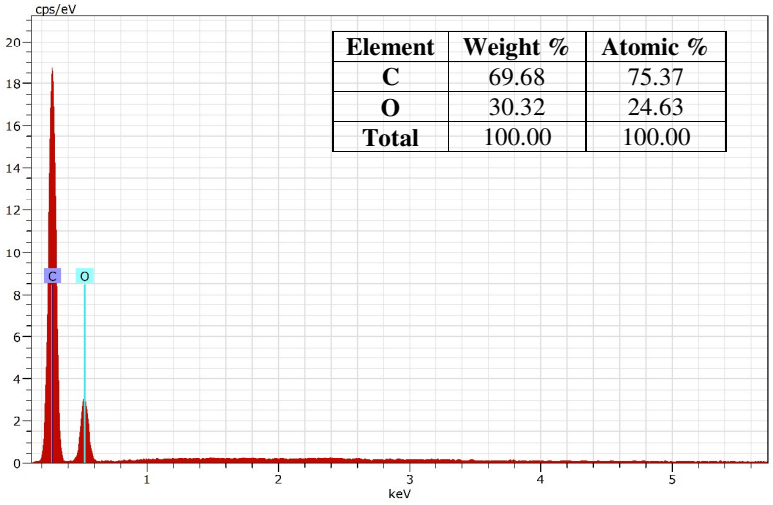

Element	Weight %	Atomic %
C	69.68	75.37
O	30.32	24.63
Total	100.00	100.00

(a)

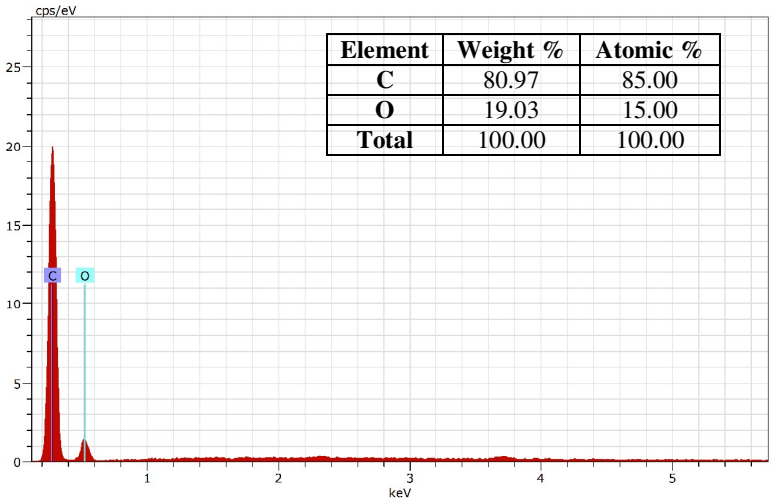

Element	Weight %	Atomic %
C	80.97	85.00
O	19.03	15.00
Total	100.00	100.00

(b)

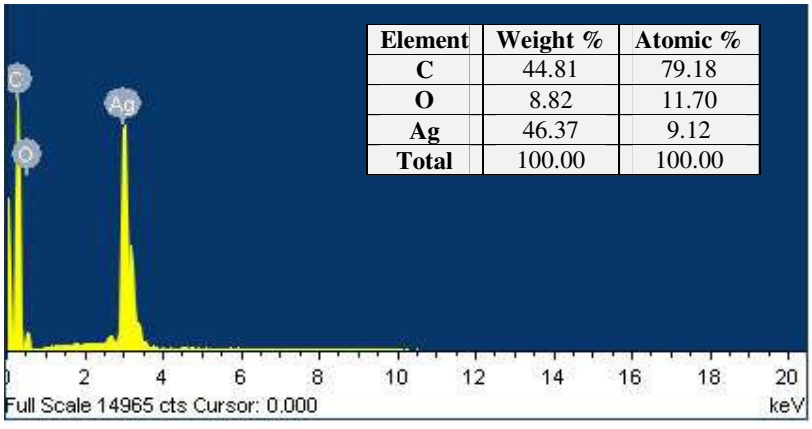

Element	Weight %	Atomic %
C	44.81	79.18
O	8.82	11.70
Ag	46.37	9.12
Total	100.00	100.00

(c)

Fig. 7 EDX spectrum of (a) graphene oxide, (b) reduced graphene oxide and (c) Ag NPs/rGO composite.

Typical features for the GO in Raman spectra (Fig. 8) are the G band around 1600 cm^{-1} and the D band around 1350 cm^{-1}. The G band is usually assigned to the first-order scattering of the E_{2g} phonons of sp^2 C atoms; the D band is the breathing mode of the k-point phonons of A_{1g} symmetry.[27] Due to the surface-enhanced Raman scattering (SERS) activity of Ag NPs,[27] both the Raman intensities of the D and G bands clearly increased for Ag NPs/rGO composite which indicates that Ag NPs have been successfully deposited on rGO sheets. The result of Raman spectra is in agreement with the previous conclusion from EDX.

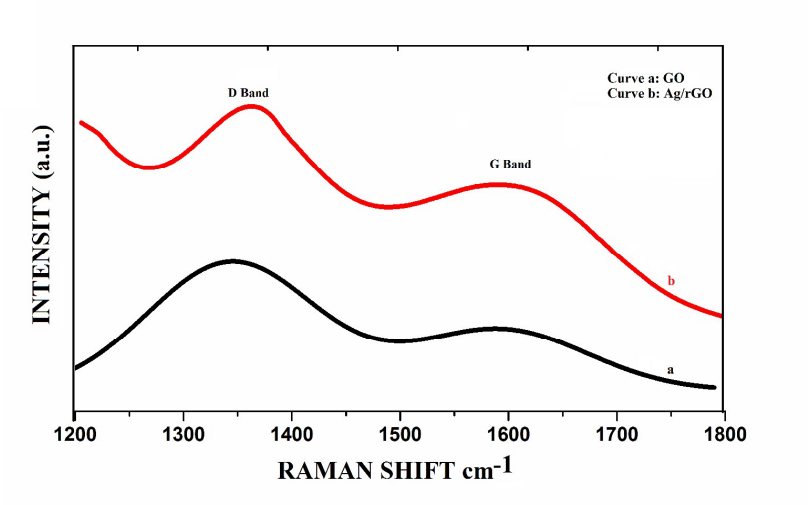

Fig. 8 Raman spectra of GO (curve a) and Ag NPs/rGO (curve b) composite.

The successful preparation of Ag NPs/rGO composite was also confirmed by UV–Vis absorption spectra. Fig. 9 shows the UV–Vis absorption spectra of GO dispersion, Ag NPs and Ag NPs/rGO composite. The UV–Vis spectrum of GO shows two peaks at 237 nm and 310 nm (low intensity) corresponding to π-n transitions of aromatic C-C bond and n-π transitions of C-O bond in GO, respectively (curve a). It can be clearly seen that the absorption peak gradually shows red-shifts from 237 to 272 nm for Ag NPs/rGO composite (curve b). Additionally, a new absorption band appears at 430 nm ascribes to the characteristic of the colloidal Ag surface plasmon resonance band, indicating the formation of Ag NPs (curve b) which is in conformity with the UV-Vis spectra of Ag NPs (curve c).

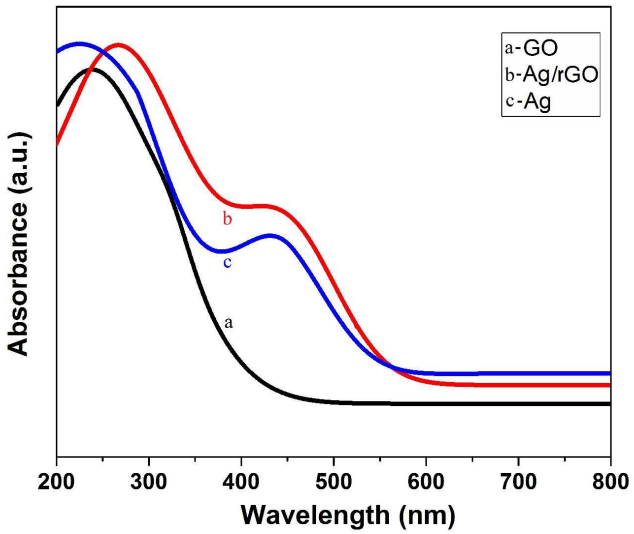

Fig. 9 UV–Vis absorption spectra of (a) GO, (b) Ag NPs/rGO composite and (c) Ag NPs.

The presence of Ag in synthesized Ag NPs/rGO composite was also confirmed by results obtained from cyclic voltammetery analysis. Fig. 10 shows the electrocatalytic responses of GO and Ag NPs/rGO composite at pH 12.0. Apparently, the response of GO is pretty weak. The Ag NPs/rGO composite shows remarkable current peak at about 7.9 µA in intensity at -0.44 V which confirmed the presence of Ag in Ag NPs/rGO composite.

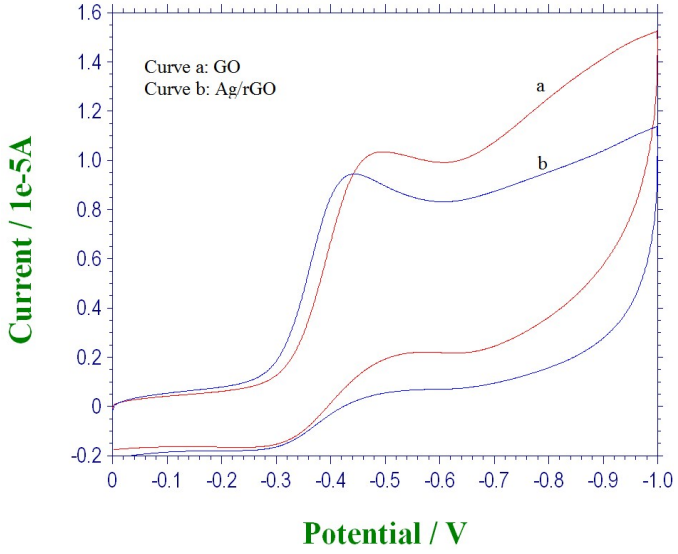

Fig. 10 Cyclic voltammetries (CVs) of GO and Ag NPs/rGO composite at pH 12.0.

FTIR spectra of GO, rGO and Ag NPs/rGO composite are shown in Fig. 11. It can be seen from FTIR spectra of GO (Fig. 11a) that the peak due to -OH stretching vibrations is observed at 3680 cm^{-1}. The peaks at 1360 cm^{-1} and 1070 cm^{-1} can be assigned to the deformation vibration of O–H and stretching vibration of C–O, respectively. Characteristic peak of C=O stretching observed at 1724 cm^{-1}. Further, a broad peak at around 1220 cm^{-1} corresponds to C–O–C vibration. Four absorption peaks from 1480 to 1630 cm^{-1} arises due to the aromatic C=C stretching of GO sheet. In the FTIR spectrum of rGO and Ag NPs/rGO composite (Fig. 11b and 11c), the peaks are relatively weak as compared to GO. The FTIR results demonstrate that the GO have been successfully exfoliated and strong interactions may exist between Ag NPs and surface functional groups of rGO sheets.[28]

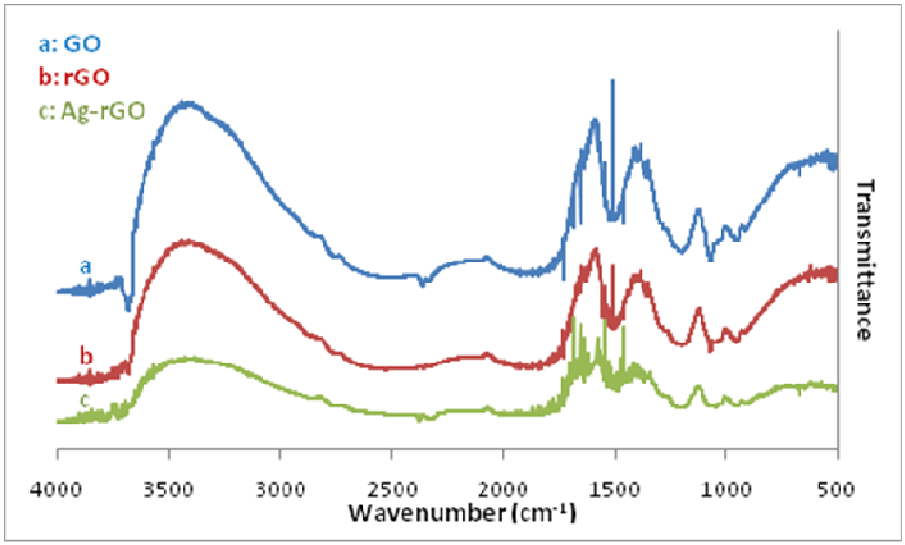

Fig. 11 FT-IR spectra of (a) GO, (b) rGO and (c) Ag NPs/rGO composite.

2.2. Catalytic performance for the chemoselective synthesis of pyrrolo[2,3,4-*kl*]acridin-1-one

At the outset of this study, our efforts were directed to find an appropriate reaction condition to perform the proposed reaction. Synthesis of pyrroloacridine derivatives from the one pot reaction involving dimedone, anilines and isatins is not straightforward, competitive formation of other products were found to be a potential problem and an issue not attended so far. The present study highlights the influence of the Ag NPs/rGO composite in controlling the selective formation of pyrroloacridine derivatives. We commenced our study by evaluating the efficiency of MW for the model reaction of isatin (2.0 mmol), dimedone (2.0 mmol) and toludene (2.0 mmol) in ethanol without using any catalyst. It was found that under

these conditions (400 W at 70 °C for 60 min.), a mixture of products is formed which is insignificant from scientific as well as economic point of view. However, the results demonstrated the need of a catalyst for selectivity in product formation. In order to set up the real effectiveness of catalyst for the chemoselective synthesis of **4b**, same model reaction was examined with different catalysts in ethanol and the results are summarized in Table 1.

Several acidic catalysts such as acetic acid, trifluoroethanol and p-TSA catalyzed the reaction with lower yields (Table 1, entry 1, 2 and 3). The use of Ag salts also showed relatively low activities (Entry 4, yield of **4b** = 31%). However, with Ag NPs the reaction proceeded smoothly to afford the corresponding product in moderate yield (Table 1, entry 5). Further experiments confirmed that GO as well as rGO sheets were also able to give good yields of the product **4b** (Table 1, entry 6 and 7). To facilitate the catalyst recovery and prevent their aggregation in reaction mixture Ag NPs were immobilized on rGO support *via* the one-pot reduction of Ag salt and GO. It was found that the best result in terms of turnover frequency (TOF: expressed as the number of moles of product produced per gram of catalyst used per min)[29] could be achieved by using Ag NPs/rGO composite as a catalyst (4 wt% loading). When the Ag NPs/rGO composite was used, the activity was settled up to (TOF) 28.16 x 10^{-3} mol g^{-1} min^{-1}. It can be imagined that, except the connection parts between Ag NPs and graphene-based sheets, most surfaces of these attached nanoparticles are exposed to the environment. Additionally, the free surface acidic groups of graphene-based sheets assist in the catalytic course of action.[30] Hence, higher catalytic activity was observed with Ag NPs/rGO composite. It is clearly revealed from Table 1 that 4 wt% of catalyst loading was sufficient to catalyze the reaction, excessive amount of catalyst did not affect the yield remarkably. Further, we have also analyzed the results in terms of amount of Ag loading in Ag NPs/rGO composite. Here, we have prepared different Ag NPs/rGO composites possessing different amount of Ag loading (According to EDX analysis 39 wt%, 46 wt%, 52 wt%). The best results were observed when we used 4 wt % of the Ag NPs/rGO composite containing 46 % of Ag loading.

Table 1. Comparison of catalytic activity of Ag NPs/rGO composite with other catalytic systems for the synthesis of pyrrolo[2,3,4-*kl*]acridin-1-one derivatives (**4b**).[a]

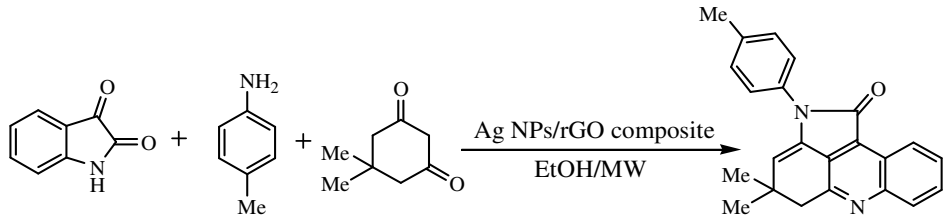

1 2b 3 4b

Entry	Condition	Time (min)	Yield(%)[b]	E-factor	TOF (x 10^{-3} mol g^{-1} min^{-1})[d]
1.	AcOH (10 wt%)	70	26	16.82	0.084
2.	TFE (10 wt%)	45	30	14.46	0.151
3.	p-TSA (10 wt%)	25	51	8.09	0.464
4.	$AgNO_3$(10 wt%)	60	31	13.95	0.118
5.	Ag NPs(10 wt%)	40	45	9.31	0.256
6.	GO (10 wt %)	30	56	7.28	0.424
7.	rGO (10 wt%)	30	53	7.76	0.401
8.	Ag NPs/rGO (10 wt%)	2	93	3.99	10.56
9.	Ag NPs/rGO (4 wt%)	2	93	3.99	28.16
10.	Ag NPs/rGO (4 wt%)[c]	70	72	7.91	0.805

[a] Reactions are performed on a 1:1:1 ratio of isatin, dimedone, toludene in EtOH under microwave irradiation (MW power 400 W at 70 °C). [b] Isolated yield. [c] In conventional condition. [d] TOF is defined as the number of moles of product produced per gram of catalyst used per min.

The superiority of ethanol as solvent as compared to other commonly employed solvents is quite clearly evident from the results summarized in Table 2. The enhanced activity of Ag NPs/rGO composite could be attributed to its good dispersion in ethanol, high Ag NPs dispersion on rGO and suitable functional groups on carbon materials.

Table 2. Effect of solvent on the synthesis pyrrolo[2,3,4-*kl*]acridin-1-one derivatives (**4b**)[a]

Entry	Solvent	Time (min)	Yield (%)[b]
1	Methanol	2	35
2	AcOH	2	55
3	Acetonitrile	2	42
4	DMF	2	18
5	THF	2	Traces of product
6	CH_2Cl_2	2	Traces of product

7	Water	2	51
8	Ethanol	2	93

[a] Reactions are performed on a 1:1:1 ratio of isatin, dimedone, toludene and 4 wt% of Ag NPs /rGO composite under microwave irradiation (MW power 400 W at 70 °C). [b] Isolated Yield

The results obtained for the synthesis of **4b** encouraged us to further explore the applicability of the Ag NPs/rGO composite for the chemoselective synthesis of pyrrolo[2,3,4-*kl*]acridin-1-one derivatives (Table 3). To study the scope and limitations of this protocol, we have employed a wide range of aryl amines (**2**) and isatins (**3**). For precursors **2** and **3** bearing either electron-donating or electron-withdrawing substituent on the aryl ring, the reactions proceeded very smoothly to provide the corresponding pyrrolo[2,3,4-*kl*]acridin-1-one derivatives (**4**). The electronic factor of aromatic ring showed almost no effect on the yields.

Table 3. Synthesis of pyrrolo[2,3,4-*kl*]acridin-1-one derivatives

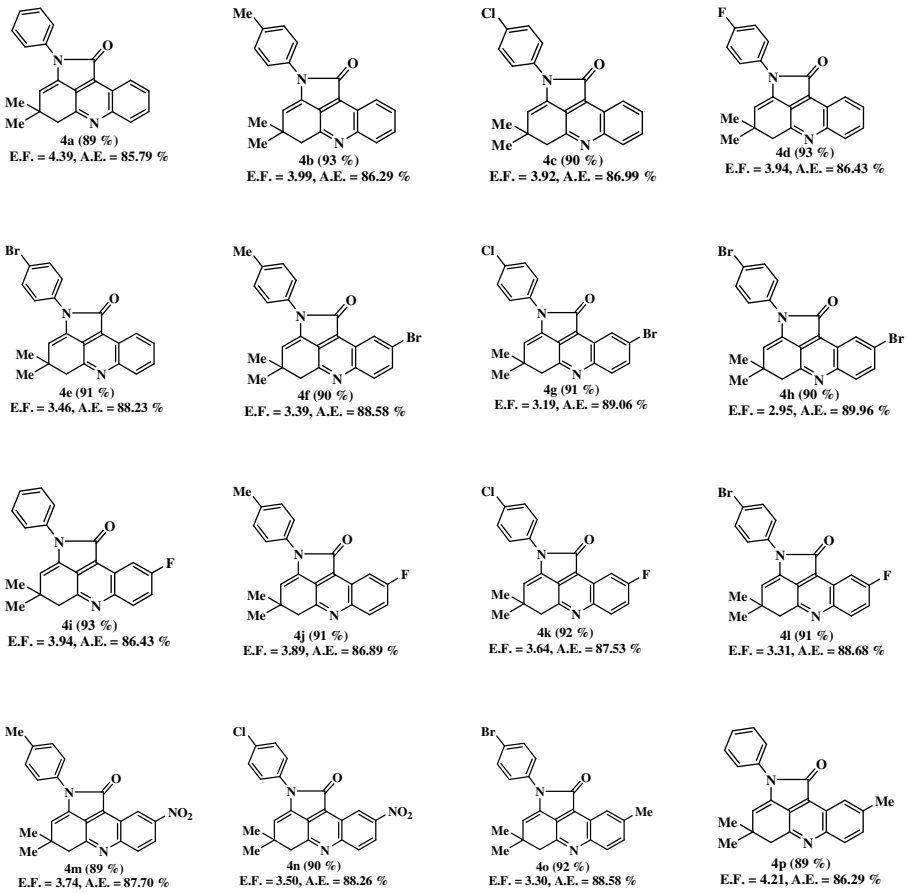

E.F. = E-factor, A.E. = Atom Economy

It is imperative to mention that the protocol is highly product selective, affording only desired product (pyrrolo[2,3,4-*kl*]acridin-1-ones); surprisingly, (1-5) (Fig. 12) were not observed in detectable amounts at all.

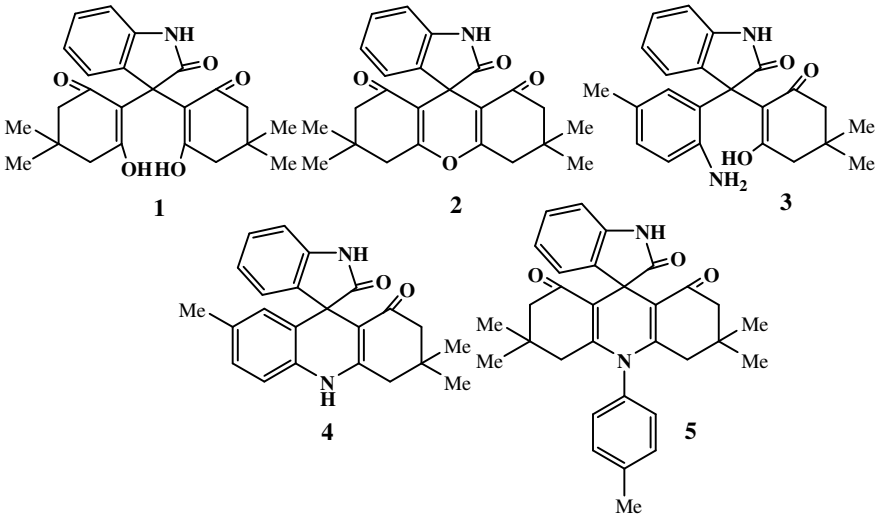

Fig. 12 Other possible products

The structure of the products 4a-p was confirmed by IR, ^{1}H, ^{13}C NMR and mass spectrometric studies. All the data were in agreement with their structures. For instance, the IR spectra of the product **4b** showed characteristic bands at 1655 cm^{-1} corresponding to the C=N group in the cyclic ring system. In ^{1}H NMR, singlet at δ 1.24 ppm was assigned to the methyl protons attached to cyclic sp^{3} C-atom. Singlet at δ 3.13 ppm was assigned to methylene protons while characteristic singlet at δ 5.51 ppm was assigned to the vinylic (=C-H) proton. Signals of eight protons of the two aromatic moieties were assigned accordingly with appropriate chemical shift value and coupling constants. The ^{13}C NMR spectrum of **4b** demonstrated signals at δ 166.8 and 137.5 ppm due to C=O and =CH-C-N group respectively in the tri cyclic ring system. The mass spectrum of **4b** showed a molecular ion peak at 340 $(M)^{+}$.

IR spectrum shows the lack of –NH group along with the appearance of a signal due to C=N in synthesized motif further ruled out the formation of other products instead of pyrrolo[2,3,4-*kl*]acridin-1-one derivatives. This was also confirmed by the ^{1}H NMR spectrum in which no signals of -NH proton was observed. Furthermore, the absence of characteristic peak of spiro carbon in ^{13}C NMR spectrum ruled out the formation of spiro products. To further confirm the structure, the X-ray diffraction analysis of the product **4b** was carried out.

As expected, the structure was pyrrolo[2,3,4-*kl*]acridin-1-one, and the concerned crystal structure is shown in Fig. 13.

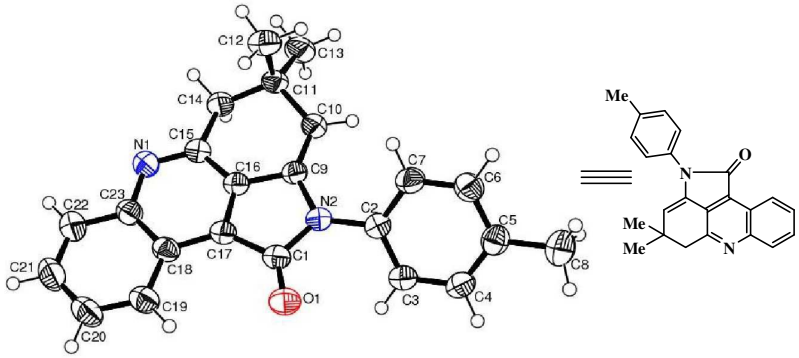

Fig. 13 Crystal structure of 4b (CCDC 1401824).

Plausible mechanism

A proposed reaction mechanism for this three-component reaction is outlined in Scheme 2. The reaction may proceed *via* any of the two possible pathways as represented in Scheme 2. Ag NPs/rGO composite can serve as an acidic catalyst for the two possible pathways (Path a and b). The literature survey reveals[23-b,c,d] that dimedone is not only a Knoevenagel reagent but also it adds easily to electron-poor olefinic bond in the Michael addition fashion leading to the formation of *bis*-hydroxy compounds. If this reaction would commence through the initial formation of Knoevenagel intermediate (**W**), then it would certainly yield other products (Path a). However, in our case pyrrolo[2,3,4-*kl*]acridin-1-one derivatives were solely obtained for all occasions. Therefore, it can be said that the reaction was not going through the Knoevenagel intermediate (**W**). A reasonable mechanism for the formation of the products was speculated with the initial formation of enaminone (**X**) catalyzed by Ag NPs/rGO composite (Path b). Then, isatin reacted with enaminone (**X**) in further step affording the intermediate (**Y**). Intermediate (**Y**) gives a new intermediate (**Z**) by losing a H_2O molecule. **Z** induces an amidic C-N bond cleavage or ring-opening sequence of isatin to give the intermediate (**Z'**). This intermediate undergoes cyclization reaction to afford the corresponding pyrrolo[2,3,4-*kl*]acridin-1-one.

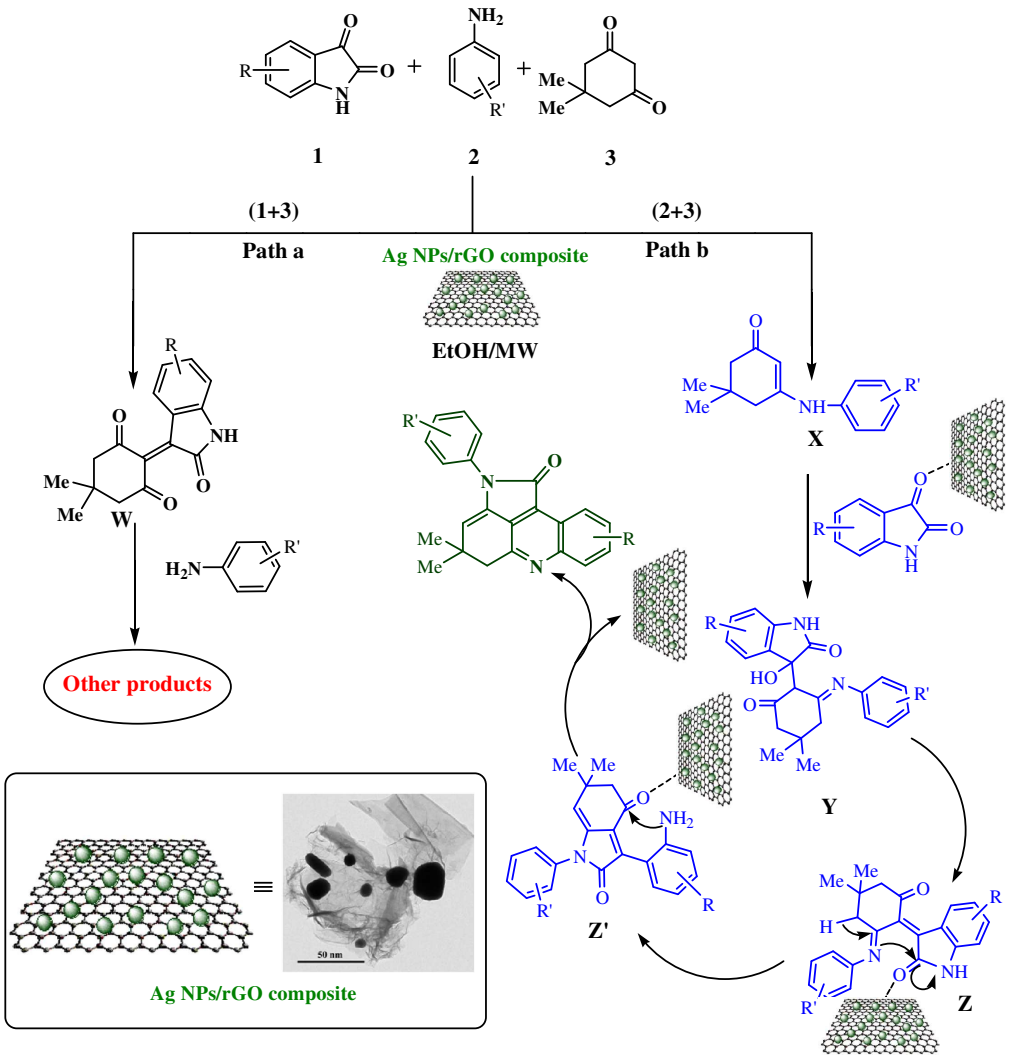

Scheme 2: Mechanistic pathway for the synthesis of pyrrolo[2,3,4-*kl*]acridin-1-one.

2.3. Heterogeneous nature and recyclability of the catalyst

The heterogeneous nature of the catalytic system was confirmed by performing the hot filtration test.[31] For this purpose, the model reaction was performed again under the optimized conditions. After 1 min, the catalyst was separated from the reaction mixture through hot filtration at approximately 40% conversion. Then the reaction was continued with the filtrate for another 25 min and conversion was monitored for every 3 min. It was observed that further increment in conversion was not observed even after 25 min. These results proved that the reaction was occurring only due to the presence of Ag NPs/rGO composite. It also showed that Ag was not detached from the catalyst during reaction. Further, ICP-AES analysis was performed on the filtrate which showed that there was no

metallic leaching in the filtrate. This whole experiment confirms the heterogeneous nature of the catalytic system and presence of strong interactions between Ag NPs and surface functional groups of rGO sheets. Therefore, it can be said that the synthesized Ag NPs/ rGO composite is quite stable and catalyze the condensation reaction of dimedone, anilines and isatins persuasively.

Recycling experiments were performed by the condensation of dimedone, toludene and isatin in ethanol as the model reaction. The reaction was carried out by using 4 wt% of catalyst and the experiments were suitably scaled up. When the reaction was completed, the resulting solid precipitate was filtered and dried along with the Ag NPs/rGO composite. Then, the solid precipitate was dissolved in acetone and the catalyst was recovered by filtration. The catalyst was washed with acetone and reused in subsequent 7 reaction cycles without any significant loss in its catalytic activity (Fig. 14).

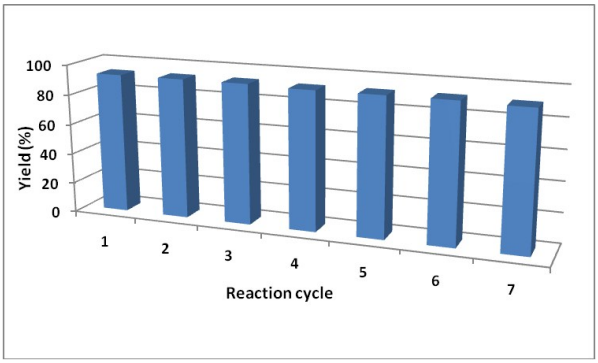

Fig. 14 Recyclability of Ag NPs/rGO composite.

3. EXPERIMENTAL SECTION

3.1. General

All the chemicals used were of research grade (purchased from Sigma Aldrich and Acros) and used without further purification. IR spectra were recorded on a Shimadzu FT IR-8400S spectrophotometer using KBr pellets. ^{1}H and ^{13}C NMR spectra were recorded in $CDCl_3$ and DMSO-d_6 using TMS as an internal standard on a Bruker spectrophotometer at 400 and 75 MHz respectively. Mass spectrum of representative compound was recorded on JEOL SX-102 spectrometer at 70 eV. The microwave-assisted reactions were carried out in a MAS-II microwave oven (2450 MHz, Sineo Microwave Chemistry Technology Company, Shanghai, China) with a maximum power output of 1000 W. This system is equipped with a power and temperature feedback control switch.

3. 2. Preparation of graphene oxide (GO)

Graphene oxide (GO) was prepared by oxidizing graphite flakes using modified Hummer's method.[32] Concentrated H_2SO_4 (69 mL) was added to 3.0 g (1 wt equiv) of graphite flakes. This mixture was cooled to 0 °C using ice bath and put on vigorous stirring for 1 hour. After that black slurry was formed. Added 1.5 g of $NaNO_3$ (0.5 wt equiv) to it slowly (in 25-30 min) and whole assembly was continued for room temperature stirring for 1 hour. Added 135 mL of water to it and stirred at 80 °C for 30 minutes. Then this material was poured into 410 mL of water with constant stirring (at room temperature). After that, 20 ml of H_2O_2 was added to it gently. The resulting mixture was filtered, washed with deionized water and centrifuged (10000 rpm for 15 min twice). The supernatant was discarded and black colored sediment was collected. This sediment was then washed with deionized water, dil. HCl and ethanol respectively. During each washing, the mixture was centrifuged (10000 rpm for 15 min) and the supernatant decanted away. The obtained black solid material was dried under vacuum for 20 h to give 1.8 g of GO.

3.3. Synthesis of Ag NPs/rGO composite

Ag NPs/rGO composite was synthesized by one-pot chemical route. Firstly, 200 mg as prepared GO was dispersed in 200 mL deionized water and ultrasonicated for 10 min using an ultrasonic probe. The obtained dispersion was centrifuged at 10000 rpm for 15 min to remove any un-exfoliated GO. Then, desired amount of $AgNO_3$ (150 mg, 200 mg and 250 mg) was dissolved in the GO dispersion and whole material was put on room temperature stirring for 30 min. After that, 20 mL hydrazine hydrate (5 mol L^{-1}) solution was added slowly to it and the mixture was shifted to reflux at 90 °C under continuous mechanical stirring for 8 h. The obtained precipitate was separated by centrifugation (10000 rpm for 15 min) and washed with deionized water, then dried under vacuum. Consequently, three sets of Ag NPs/rGO composites were obtained containing different amount of Ag loading (39 wt%, 46 wt%, 52 wt%). For comparison, we have also prepared rGO (without Ag) by the reduction of GO by same procedure without using $AgNO_3$.

3.4. Catalyst characterization

The size and morphology of the synthesized material was observed by transmission electron microscopy (TEM) using a JEOL 1011 at an accelerating voltage of 200kV. X-ray diffraction (XRD) measurements for phase determination were recorded by Philips powder diffractometer (PW3040/60) with Cu K_α radiation (1.54060nm) operating in a continuous mode to collect 2θ values with a scan rate of 0.02°/min. SEM and EDX measurements of the synthesized material was performed using a FEI Quanta 200F SEM and Bruker SEM fitted

with an EDX. X-ray photoelectron spectra (XPS) were measured on a commercial SPECS spectrometer (Germany), equipped with an Al-Kα X-ray source (1486.5eV). The UV-Vis spectra were recorded using Ocean optics USB 2000 spectrophotometer in the solution form. All electrochemical experiments were performed with a CHI electrochemical analyzer, USA model no. 1230A (SR 400). The Raman spectra were recorded by micro-Raman spectrometer (Jobin Yvon Horibra LABRAM-HR visible 400-1100 nm).

3.5. General procedure for the synthesis of pyrrolo[2,3,4-*kl*]acridin-1-one derivatives

Isatin (2 mmol), dimedone (2 mmol), aniline derivative (2 mmol) and 4 wt% of Ag NPs/rGO composite (4 wt% with respect to the reactants used: see ESI) in ethanol (3 mL) was introduced in a 10 mL round-bottom flask. The flask was placed in the microwave cavity and the reaction mixture was irradiated at 70 $^{\circ}$C for 2 min. using a maximum power of 400W. The complete conversion of the starting materials into products was checked and proved by TLC (Benzene: Ethyl acetate- 8:2). When the reaction was completed, the resulting solid precipitate was filtered and dried along with the catalyst. Then, the solid precipitate was dissolved in acetone and the catalyst was recovered by filtration. This solution was concentrated at room temperature to generate the crude product. The crude product was purified by crystallization from ethanol.

4. Conclusions

In summary, we have demonstrated that catalytically active Ag NPs/rGO composite can be prepared by a facile and scalable chemical route. The results from TEM, XRD, SEM, XPS, EDX, UV–Vis, cyclic voltammetery, Raman and FT-IR spectra proved that method was a feasible and reliable route to reduce GO and prepare Ag NPs on its surface *via* one pot process. The successful in situ growth of Ag NPs onto the surface of rGO leads to the formation of stable nano-material Ag NPs/rGO composite with remarkable and durable catalytic activity for the chemoselective synthesis of pyrrolo[2,3,4-*kl*]acridin-1-ones *via* the one pot reaction of dimedone, various anilines and isatins in ethanol. The reaction proceeds *via* amidic C-N bond cleavage or ring-opening sequence of isatin and showed remarkable selectivity for pyrrolo[2,3,4-*kl*]acridin-1-ones over other products. The catalytic activity of Ag NPs/rGO composite was about 35-fold higher under microwave irradiation as compared to conventional techniques. The catalyst was very stable and could be easily separated from the products and reused for 7 times with superior activity. Excellent results were obtained when the reactions were analyzed using green chemistry metrics.

Acknowledgments

Financial assistance from the CSIR and UGC, New Delhi, India are gratefully acknowledged. We are thankful to the National Facility for Drug Discovery Complex, Saurashtra University, Rajkot, India for the spectral analyses. We are also thankful to Dr. Shaikh M. Mobin, Assistant Professor and In-charge Sophisticated Instrument Centre (SIC), IIT Indore, India for single crystal X-ray analysis.

References:

1. (a) N. Arumugam, R. Raghunathan, A. I. Almansour and U. Karama, *Bioorg. Med. Chem. Lett.,* 2012, **22**, 1375-1379; (b) S. Jiang, H. Lu, S. Liu, Q. Zhao, Y. He and A. K. Debnath, *Antimicrob. Agents Chemother.,* 2004, **48**, 4349-4359; (c) G. H. Jana, S. Jain, S. K. Arora and N. Sinha, *Bioorg. Med. Chem. Lett.,* 2005, **15**, 3592-3595; (d) K. J. Kim, M. J. Choi, J.-S. Shin, M. Kim, H.-E. Choi, S. M. Kang, J. H. Jin, K.-T. Lee and J. Y. Lee, *Bioorg. Med. Chem. Lett.,* 2014, **24**, 1958-1962; (e) J. C. Arnould, B. Delouvrie, P. Boutron, A. G. Dossetter, K. M. Foote, A. Hamon, U. Hancox, C. S. Harris, M. Hutton, M. Lamorlette and Z. Matusiak, *Bioorg. Med. Chem. Lett.,* 2007, **17,** 6448-6454.
2. N. P. Gaponik, D. V. Talapin, A. L. Rogacha and A. Eychmuller, *J. Mater. Chem*., 2000, **10**, 2163-2166.
3. (a) M. Wainwright, *J. Antimicrob. Chemother*., 2001, **47**, 1-13; (b) S. A. Gamage, D. P. Figgitt, S. J. Wojcik, R. K. Ralph, A. Ransijn, J. Mauel, V. Yardley, D. Snowdon, S. L. Croft and W. A. Denny, *J. Med. Chem.,* 1997, **40**, 2634-2642; (c) P. M. Chauhan and S. K. Srivastava, *Curr. Med. Chem.,* 2001, **8**, 1535-1542.
4. J. Stanslas, D. J. Hagan, M. J. Ellis, C. Turner, J. Carmichael, W. Ward, T. R. Hammonds, and M. F. G. Stevens, *J. Med. Chem.,* 2000, **43**, 1563-1572.
5. (a) S. Fukuzumi, Y. Tokuda, T. Etano, T. Okamoto and J. Otera, *J. Am. Chem. Soc.,* 1993, **115**, 8960-8968; (b) N. Bensel, N. Bahr, M. T. Reymond, C. Schenkels and J.-L. Reymond, *Helv. Chim. Acta,* 1999, **82**, 44-52.
6. (a) W. D. Inman, M. O'Neill-Johnson and P. Crews, *J. Am. Chem. Soc.*, 1990, **112**, 1-4; (b) A. Kamal, O. Srinivas, P. Ramulu, G. Ramesh and P. Praveen Kumar, *Bioorg. Med. Chem. Lett.,* 2004, **14,** 4107-4111; (c) E. Gimenez-Arnau; S. Missailidis and M. F. G. Stevens, *Anti-Cancer Drug Des.,* 1998, **13**, 431-451.
7. (a) R. R. West, C. L. Mayne, C. M. Ireland, L. S. Brinen and J. Clardy, *Tetrahedron Lett.*, 1990, **31**, 3271-3274; (b) C. J. Smith, D. A. Venables, C. Hopmann, C. E. Salomon, J. Jompa, A. Tahir, D. J. Faulkner and C. M. Ireland, *J. Nat. Prod.*, 1997, **60**, 1048-1050; (c) Z. Thale, T. Johnson, K. Tenney, P. J. Wenzel, E. Lobkovsky, J. Clardy, J. Media, H. Pietraszkiewicz, F. A. Valeriote and P. Crews, *J. Org. Chem.*, 2002, **67**, 9384-9391; (d) P. Ralifo, L. Sanchez, N. C. Gassner, K. Tenney, R. S. Lokey, T. H. Holman, F. A. Valeriote and P. Crews, *J. Nat. Prod.*, 2007, **70**, 95-99.
8. (a) A. W. and J. Lhomme, *Tetrahedron Lett.,* 1993, **34**, 6411-6414; (b) G. Gellerman, A. Rudi and Y. Kashman, *Tetrahedron,* 1994, **50**, 12959-12972; (c) M. A. Munawar and P.

W. Groundwater, *Bull. Korean Chem. Soc*., 1999, **20**, 456-458; (d) Y. Kitahara, T. Mizuno and A. Kubo, *Tetrahedron*, 2004, **60**, 4283-4288; (e) R. Meesala and R. Nagarajan, *Tetrahedron Lett.*, 2010, **51**, 422-424; (f) H. Wang, L. Li, W. Lin, P. Xu, Z. Huang and D. Shi, *Org. Lett.,* 2012, **14**, 4598-4601; (g) W.-J. Hao, J.-Q. Wang, X.-P. Xu, S.-L. Zhang, S.-Y. Wang and S.-J. Ji, *J. Org. Chem.,* 2013, **78**, 12362-12373; (h) C. Cao, C. Xu, W. Lin, X. Li, M. Hu, J. Wang, Z. Huang, D. Shi, and Y. Wang, *Molecules,* 2013, **18**, 1613-1625.

9. H. Kefayati, F. Narchin and K. Rad-Moghadam, *Tetrahedron Lett.,* 2012, **53**, 4573-4575.
10. (a) R. P. Swatloski, J. D. Holbrey and R. D. Rogers, *Green Chem.*, 2003, **5**, 361-363; (b) M. T. Garcia, N. Gathergood and P. J. Scammells, *Green Chem.,* 2005, **7**, 9-14; (c) M. Uerdingen, C. Treber, M. Balser, G. Schmitt and C. Werner, *Green Chem.,* 2005, **7**, 321-325; (d) D. Zhao, Y. Liao and Z. Zhang, *Clean,* 2007, **35**, 42-48; (e) Y. Deng, I. Beadham, M. Ghavre, M. F. C. Gomes, N. Gathergood, P. Husson, B. Légeret, B. Quilty, M. Sancelmea, and P. Besse-Hoggan, *Green Chem.,* 2015, **17**, 1479-1491.
11. (a) V. Hessel, D. Kralisch and U. Krtschil, *Energy Environ. Sci.,* 2008, **1**, 467-478; (b) M. M. Kirchhoff, *Resour. Conserv. Recy.*, 2005, **44**, 237-243.
12. (a) R. S. Varma and D. Kumar, *Tetrahedron Lett.,* 1999, **40**, 7665-7669; (b) V. Polshettiwar and R. S. Varma, *J. Org. Chem.*, 2007, **72**, 7420-7422; (c) P. Kaswan, K. Pericherla, H. K. Saini and A. Kumar, *RSC Adv.*, 2015, **5**, 3670-3677.
13. (a) J. H. Schrittwieser, F. Coccia, S. Kara, B. Grischek, W. Kroutil, N. d'Alessandrod and F. Hollmann, *Green Chem.,* 2013, **15**, 3318-3331; (b) R. C. Cioc, E. Ruijter and R. V. A. Orru, *Green Chem.,* 2014, **16**, 2958-2975.
14. (a) C.-L. Lee, C.-H. Huang, K.-L. Huang, Y.-L. Tsai and C.-C. Yang, *Carbon*, 2013, **60**, 392-400; (b) N. Xiao, Y. Zhou, Z. Ling, Z. Zhao and J. Qiu, *Carbon,* 2013, **60**, 514-522.
15. (a) D. R. Dreyer, S. Park, C. W. Bielawski and R. S. Ruoff, *Chem. Soc. Rev.,* 2010, **39**, 228-240; (b) J. I. Paredes, S. Villar-Rodil, M. J. Fernandez-Merino, L. Guardia, A. Martınez-Alonso and J. M. D. Tascon, *J. Mater. Chem.,* 2011, **21**, 298-306; (c) C. K. Chua and M. Pumera, *Chem. Soc. Rev.,* 2014, **43**, 291-312.
16. (a) M. Pumera, *Chem. Soc. Rev.,* 2010, **39**, 4146-4157; (b) Y. Lin, J. Jin and M. Song, *J. Mater. Chem.,* 2011, **21**, 3455-3461; (c) G. Zhao, T. Wen, C. Chen and X. Wang, *RSC Adv.,* 2012, **2**, 9286-9303; (d) E. Farjami, M. A. Rottmayer and L. J. Deiner, *J. Mater. Chem. A,* 2013, **1**, 15501-15508.
17. (a) R. Nie, J. Wang, L. Wang, Y. Qin, P. Chen and Z. Hou, *Carbon,* 2012, **50**, 586-596; (b) Y. Zheng and A. Wang, *J. Mater. Chem.,* 2012, **22**, 16552-16559; (c) P. Wang, Z.-G.

Liu, X. Chen, F.-L. Meng, J.-H. Liu and X.-J. Huang, *J. Mater. Chem. A,* 2013, **1**, 9189-9195; (d) X. Ran, H. Sun, F. Pu, J. Ren and X. Qu, *Chem. Commun.,* 2013, **49**, 1079-1081.

18. (a) Y. Mikami, A. Noujima, T. Mitsudome, T. Mizugaki, K. Jitsukawa and K. Kaneda, *Tetrahedron Lett.,* 2010, **51**, 5466-5468; (b) K. Seth, S. R. Roy, D. N. Kommi, B. V. Pipaliya and A. K. Chakraborti, *J. Mol. Catal. A: Chem.,* 2014, **392**, 164-172; (c) L.-Q. Zheng, X.-D. Yu, J.-J. Xu and H.-Y. Chen, *Chem. Commun.,* 2015, **51**, 1050-1053.
19. (a) H. Cong, C. F. Becker, S. J. Elliott, M. W. Grinstaff, and J. A. Porco Jr, *J. Am. Chem., Soc*. 2010, **132**, 7514-7518; (b) R. Mohammadi, E. Eidi, M. Ghavami and M. Z. Kassaee, *J. Mol. Cat. A: Chem.*, 2014, **393**, 309-316.
20. (a) A. E. E. A. Ragab, A. Gadallah, M. B. Mohamed and I. M. Azzouz, *Opt. Laser Technol.*, 2013, **52**, 109-112; (b) E. K. Goharshadi and H. Azizi-Toupkanloo, *Powder Technol.*, 2013, **237**, 97-101; (c) Y. Li, Y. Wu and B. S. Ong, *J. Am. Chem. Soc.,* 2005, **127**, 3226-3227.
21. (a) A. M. Abdelgawad, S. M. Hudson and O. J. Rojas, *Carbohydr. Polym.*, 2014, **100**, 166-178; (b) L. Balogh, D. R. Swanson, D. A. Tomalia, G. L. Hagnauer and A. T. McManus, *Nano Lett.*, 2001, **1**, 18-21; (c) J. E. Gray, P. R. Norton, R. Alnouno, C. L. Marolda, M. A. Valvano and K. Griffiths, *Biomaterials*, 2003, **24**, 2759-2765; (d) B. Pant, H. R. Pant, D. R. Pandey, G. Panthi, K. T. Nam, S. T. Hong, C. S. Kim and H. Y. Kim, *Colloids Surf. A: Physicochem. Eng. Asp.*, 2012, **395**, 94-99.
22. (a) A. Dandia, A. K. Jain and D. S. Bhati, *Tetrahedron Lett.,* 2011, **52**, 5333-5337; (b) A. Dandia, V. Parewa, A. K. Jain and K. S. Rathore, *Green Chem.* 2011, **13**, 2135-2145; (c) A. Dandia, A. K. Jain and S. Sharma, *Tetrahedron Lett.,* 2012, **53**, 5859-5863; (d) A. Dandia, A. K. Jain and S. Sharma, *Tetrahedron Lett.,* 2012, **53**, 5270-5274; (e) A. Dandia, V. Parewa and K. S. Rathore, *Catal. Comm.,* 2012, **28**, 90-94; (f) A. Dandia, A. K. Jain, D. S. Bhati and A. K. Laxkar, *Tetrahedron,* 2013, **69**, 2062-2069; (g) A. Dandia, V. Parewa, S. L. Gupta and K. S. Rathore, *J. Mol. Catal. A: Chem.,* 2013, **373**, 61-71; (h) A. Dandia, V. Parewa, S. Maheshwari and K. S. Rathore, *J. Mol. Catal. A: Chem.,* 2014, **394**, 244-252; (i) A. Dandia, V. Parewa, S. L. Gupta, A. Sharma and N. K. Agarwal, *Curr. Org. Chem.*, 2014, **18**, 2652-2664; (j) A. Dandia, V. Parewa, S. L. Gupta, A. Sharma, K. S. Rathore, A. Sharma and A. Jain, *Catal. Comm.*, 2015, **61**, 88-91.
23. (a) S. Ahadi, H. R. Khavasi and A. Bazgir, *Chem. Pharm. Bull.* 2008, **56**, 1328-1330; (b) K. C. Joshi, R. Jain and S. Arora, *J. Fluorine Chem.,* 1989, **42**, 149-162; (c) M. Dabiri, M. Bahramnejad and M. Baghbanzadeh, *Tetrahedron*, 2009, **65**, 9443-9447; (d) R.

Ghahremanzadeh, S. Ahadi, G. I. Shakibaei and A. Bazgir, *Tetrahedron Lett.*, 2010, **51**, 499-502; (e) A. Bazgir, S. Ahadi, R. Ghahremanzadeh, H. R. Khavasi and P. Mirzaei, *Ultrason. Sonochem.,* 2010, **17**, 447-462; (f) A. R. Khorrami, F. Faraji and A. Bazgir, *Ultrason. Sonochem.,* 2010, **17**, 587-591.

24. X. Chao and W.Xin, *Small,* 2009, **19**, 2212-2217.
25. (a) J. I. Paredes, S. Villar-Rodil, P. Solis-Fernandez, A. Martinez-Alonso and J. M. D. Tascon, *Langmuir*, 2009, **25**, 5957-5968; (b) M. F. Lengke, M. E. Fleet and G. Southam, *Langmuir,* 2007**, 23***,* 2694-2699; (c) S. Kundu, D. Huitink, K. Wang and H. Liang, *J. Colloid Interface Sci.*, 2010, **344**, 334**–**342.
26. (a) C. Xu, X. Wang, L. Yang, Y. Wu, *J. Solid State Chem*., 2009, **182**, 2486-2490; (b) T. A. Pham, B. C. Choi and Y. T. Jeong, *Nanotechnology*, 2010, **21,** 465603; (c) Q. Bao, D. Zhang and P. Qi, *J. Colloid Interface Sci.*, 2011, **360**, 463-470; (d) W. L. Zhang and H. J. Choi, *Langmuir*, 2012, **28**, 7055-7062.
27. (a) J. Gao, F. Liu, N. Ma, Z. Wang and X. Zhang, *Chem. Mater.*, 2010, **22**, 2213- 2218; (b) A. Maoa, D. Zhang, X. Jin, X. Gu, X. Wei, G. Yang and X. Liu, *J. Phys. Chem. Solids*, 2012, **73**, 982-986.
28. (a) J. Yang, C. Zang, L. Sun, N. Zhao and X. Cheng, *Mater. Chem. Phys.,* 2011, **129***,* 270-274; (b) C. Xu and X. Wang, *Colloids Surf. A: Physicochem. Eng. Asp.,* 2012, **404**, 78-82; (c) W. Yuan, Y. Gu and L. Li, *Appl. Surf. Sci.,* 2012, **261**, 753-758; (d) Y. Han, Z. Luo, L. Yuwen, J. Tian, X. Zhu and L. Wang, *Appl. Surf. Sci.,* 2013, **266**, 188-193.
29. D. R. Dreyer, H.-P. Jia, and C. W. Bielawski, *Angew. Chem.*, 2010, **122**, 6965-6968.
30. H.-P. Jia, D. R. Dreyer and C. W. Bielawski , *Tetrahedron*, 2011, **67**, 4431-4434.
31. S. Nojima, K. Kamata, K. Suzuki, K. Yamaguchi and N. Mizuno, *ChemCatChem,* 2015, **7***,* 1097–1104.
32. W. S. J. Hummers and R. E. Offeman, *J. Am. Chem. Soc.*, 1958, **80**, 1339-1339.